

Delayed Excimer Fluorescence of Fluoranthene Due to Triplet-Triplet Annihilation: Systematic Study of the Fluorescence from a Weakly Bound Excimer

By Miriam Gehring and Bernhard Nickel*

Max-Planck-Institut für Biophysikalische Chemie, Abteilung Spektroskopie und
Photochemische Kinetik, Am Fassberg 11, D-37077 Göttingen, Germany

*Dedicated to Prof. Dr. Dr. h.c. mult. Jürgen Troe
on the occasion of his 60th birthday*

(Received August 10, 2000; accepted August 15, 2000)

Excimer / Delayed Fluorescence / Triplet-Triplet Annihilation / Kinetic Model / Smoluchowski Equation

Solutions of fluoranthene exhibit a delayed fluorescence (DF) due to triplet-triplet annihilation, $^3M^* + ^3M^* \rightarrow ^1M^* + ^1M$ (P-type DF). In the fluid solvent 3-methylpentane, at low temperatures, the DF consists of two components: delayed monomer fluorescence (DMF) and a slightly red-shifted component, which is assigned to delayed excimer fluorescence (DEF). The temperature dependence of the intensity ratio Q_{EM} of DEF and DMF was measured between 133 K and 293 K. The assignment of the second component of the DF to the DEF of fluoranthene is consistent with the rise and the decay of the DF at 153 K. A kinetic model was developed that describes the reversible geminate association of a $^1M^* \cdots ^1M$ pair to an excimer, $^1M^* \cdots ^1M \rightleftharpoons ^1(MM)^*$. The main features of the kinetic model are: a Smoluchowski equation, a distance-dependent relative diffusion coefficient, an exponential distance dependence of the first-order rate coefficient for the annihilation of a triplet pair, and a short-range potential representing the excimer. The Smoluchowski equation was numerically solved with a new algorithm, which is based on numerical fundamental solutions and allows the successive doubling of the total diffusion time. The kinetic model accurately describes $Q_{EM}(T)$ from ≈ 150 K (maximum of $Q_{EM}(T)$) to room temperature. The effective first-order rate constant for excimer dissociation, $k_{diss}(T)$, the equilibrium constant $K_{EM}(T)$ for excimer formation, and the excimer binding enthalpy are estimated. The observability of prompt excimer fluorescence is discussed. A formation enthalpy of the ground-state dimer of $\approx -hc \times 500 \text{ cm}^{-1}$ is estimated. The major part of the DEF spectrum is approximately equal to a spectrum, which is produced by inhomogeneous spectral broadening (i.e. convolution with a Gaussian) and a red-shift

* Corresponding author. E-mail: bnickel@gwdg.de

of the spectrum of the monomer fluorescence. The DEF spectrum contains no band that corresponds to the 0-0 transition of the monomer fluorescence.

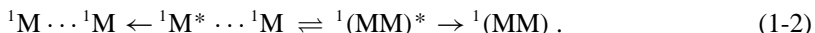
1. Introduction

In the literature on excimers of aromatic compounds prevails the idea that the spectrum of an excimer fluorescence is always structureless and differs completely from the spectrum of a monomer fluorescence [1–8]. This idea is based on a potential energy diagram, in which the interaction potential between two molecules in their electronic ground states is completely repulsive [1, 2]. Thus, according to this potential energy diagram, the excimer fluorescence would be a transition from a bound dimer state to a continuum of non-bound dimer states. The assumption of a purely repulsive potential in the electronic ground state is in contradiction to the universal van-der-Waals interaction in general and to the mutual attraction of molecules in molecular crystals in particular. A more realistic potential energy diagram was introduced by Warshel and Huler in 1974 [9]. According to their diagram, the intermolecular interaction potential is attractive also in the ground state; relative to the excited-state potential minimum, the ground-state potential minimum is less deep and at a slightly greater intermolecular distance. With strongly bound excimers, the absence of spectral structure is a consequence of the participation of intermolecular vibrational modes in the emission of excimer fluorescence. The particularly attractive aspect of this model is that the lack of spectral structure is no longer a necessary feature of excimer fluorescence: The spectrum of the excimer fluorescence becomes similar to that of the monomer fluorescence when the excimer interaction potential becomes similar to that of a ground-state dimer with the same relative molecular orientation.

On the basis of the preceding consideration it makes sense to search for the excimer fluorescence from compounds like phenanthrene or fluoranthene, which are conventionally regarded as compounds that do not form excimers. The spectrum, the quantum yield, and the lifetime of the prompt fluorescence from liquid solutions of phenanthrene [10, 11] or fluoranthene [12, 13] are nearly independent of the solute concentration. The usual procedure for the determination of the spectrum of the excimer fluorescence, which is based on the comparison of prompt-fluorescence spectra measured with different concentrations of the solute, cannot be applied, because the concentration dependence of the spectrum of the prompt monomer fluorescence is no longer negligible at the required high solute concentrations. The best way for the unambiguous detection of excimer fluorescence is the investigation of the delayed fluorescence in fluid solution at low temperatures, which is caused by excitation of ground-state molecules 1M to the first excited singlet state $^1M^*$, intersystem crossing $^1M^* \rightsquigarrow ^3M^*$, and subsequent triplet-triplet annihilation (TTA) [14, 15],



In fluid solution, the primary ${}^1M^* \dots {}^1M$ pair formed by TTA can either dissociate and emit monomer fluorescence, ${}^1M^* \rightarrow {}^1M$, or associate to an excimer, ${}^1(MM)^*$, and emit excimer fluorescence ${}^1(MM)^* \rightarrow {}^1(MM)$:



In fluid solution and in the spectral range of the fluorescence from the lowest excited singlet state, the spectrum of delayed monomer fluorescence (DMF) is virtually identical with the spectrum of prompt monomer fluorescence. Therefore the spectrum of the delayed excimer fluorescence (DEF) can be obtained by subtracting the spectrum of the prompt monomer fluorescence from the spectrum of the total delayed fluorescence. Apart from the spectrum of the DEF, the quantity of main interest is the ratio

$$Q_{EM} = I_{DEF}/I_{DMF} \quad (1-3)$$

of the spectrally integrated intensities I_{DEF} and I_{DMF} of DEF and DMF, respectively.

Earlier studies of the delayed fluorescence from fluoranthene in methylcyclohexane at 193 K [16] and from phenanthrene in perfluorohexane at 200 K [17] indeed revealed significant differences between the spectra of prompt fluorescence and delayed fluorescence. For a systematic study of the DEF, fluoranthene has the advantage that the DEF can be safely distinguished from the DMF due to the absence of a distinct 0-0 transition in the spectrum of the DEF. The measurement of the intensity ratio Q_{EM} of fluoranthene in a large temperature range was the first main objective of the present study.

Typically the temperature-dependent intensity ratio $Q_{EM}(T)$ has a maximum [18–20]. The decrease of Q_{EM} below T_{max} is caused predominantly by the increasing viscosity of the solvent: The mean intermolecular distance, at which TTA takes place, increases and the probability of geminate excimer formation decreases with decreasing temperature. The decrease of Q_{EM} above T_{max} is caused mainly by the increasing probability of thermally activated excimer dissociation. As Butler and Pilling [21] have shown, quantitative information on the distance dependence of TTA can be extracted from the low-temperature range of Q_{EM} by applying an adequate kinetic model to the experimental data. In the present paper it will be shown that, by kinetic modeling of the whole temperature range of Q_{EM} , also information on the properties of the excimer can be obtained; in particular, the equilibrium constant, the binding enthalpy B_E and the dissociation rate constant can be determined. By the combination of B_E with spectral data, the formation enthalpy of the ground-state dimer can be estimated. The development of an adequate kinetic model has been the second main objective of this study.

Finally, the present use of the term *excimer* is to be specified. The terms *excited dimer* and *excimer* are used as synonyms. The usual distinction between the two terms will be discussed in Sect. 6.6.

2. Experimental

The experimental technique has been essentially the same as described in [22].

Substances

The fluoranthene was of the same quality as in previous work [16, 17] (the purification procedure is described in [16]). The solvent 3-methylpentane was rectified over a 1-m column and chromatographed with basic aluminium oxide before use.

Sample

The sample consisted of a glass apparatus with a fluorescence flow cell through which about 200 ml of a degassed solution of fluoranthene ($2 \cdot 10^{-5}$ mol dm⁻³) in 3-methylpentane circulated (cf. Fig. 3 in [22]). The temperature of the solution was measured with a thermocouple close to the fluorescence flow cell (behind the flow cell with respect to the flow direction). The temperature was kept constant to ± 0.5 K. The estimated maximum uncertainty of the absolute temperature is ± 2 K at the lowest temperature. Practically the fluorescence could be measured in a temperature range corresponding to a solvent viscosity $\lesssim 20$ mPa s. The main advantages of this fluorescence cell are the avoidance of local heating due to excitation and the virtual elimination of disturbing effects of photoproducts. The main disadvantages are a restriction to solvents of low or moderate viscosity and a deviation of the measured decay of a delayed fluorescence from the true decay due to the moving solution (the latter effect remains small, however, if the decay time of the delayed fluorescence is short, e.g. of the order of a few milliseconds).

Excitation

The excitation light source was an argon ion laser (Spectra Physics, model 2045-15/3.5S, specified power 3.5 W in the near UV). The UV lines were externally separated with a silica Brewster prism, and the incompletely separated UV lines at 333.6 and 334.5 nm were used for excitation.

Prompt and delayed fluorescence

The spectra of the total delayed fluorescence (DF) and of the prompt fluorescence (PF) were measured with the same sample at the same temperature. All luminescence spectra were corrected for intensity fluctuations (see below) and the spectral sensitivity of the spectrometer. Both spectra were approximately normalized to equal intensity in the 0-0 transition of the $S_1 \rightarrow S_0$ fluorescence at 406 nm. The criteria for the correct normalization factor were the absence of structure and an almost vanishing intensity in the difference spectrum at the 0-0 transition of the PF at 406 nm. In the spectral range between the 0-0 transitions of the phosphorescence at 540 nm and of the monomer fluorescence at 406 nm,

the difference spectrum of the two normalized spectra is equal to the spectrum of delayed excimer fluorescence (DEF).

Correction for intensity fluctuations

The determination of sufficiently accurate difference spectra required a sufficient long-term stability of the experimental setup and an adequate correction for intensity fluctuations. In the usual correction method, the fluorescence spectrum $F(\lambda)$ and the intensity of the excitation light $I_{\text{exc}}(\lambda)$ belonging to the fluorescence wavelength λ are simultaneously recorded and the ratio $F(\lambda)/I_{\text{exc}}(\lambda)$ is calculated. This method does not work, when F is not proportional to I_{exc} , as in the case of a delayed fluorescence due to TTA, where $F \propto (I_{\text{exc}})^n$ with $1 < n < 2$; the limits correspond to a strongly dominant contribution ($n \approx 1$) or very small contribution ($n \approx 2$) of TTA to the total triplet decay. We assume that the spectrum of the delayed fluorescence is not changed by a fluctuation of the excitation light, i.e. we assume that the whole spectrum fluctuates, but not its relative intensity distribution. Then the intensity fluctuations can be corrected for by simultaneously measuring the fluorescence spectrum $F(\lambda)$ and the time dependence of the fluorescence intensity at a fixed wavelength λ_{fix} , $F(\lambda_{\text{fix}}, \lambda)$. The measurement of $F(\lambda_{\text{fix}}, \lambda)$ was realized as follows. The fluorescence light was dispersed in a grating double monochromator that contained a 90° plane deflection mirror between the entrance slit and the first spherical collimating mirror (in Fig. 4 of [22] at the right side of slit Sl_3). The aluminium-coated plane mirror had two transparent stripes. The small fraction of the undispersed fluorescence light that was transmitted by the transparent stripes passed an interference filter (and, if necessary, a neutral-density filter for additional attenuation) and was measured with a second photomultiplier. The only restriction to the wavelength λ_{fix} was that it should be below the origin of the phosphorescence. In practice an interference filter with maximum transmission at the fluorescence maximum was used.

Photomultipliers

For the long-term stability of the sensitivity of the photomultipliers, three details were important. (1) Constancy of applied high voltage. (2) A constant temperature of the photomultiplier tube, which was achieved by temperature-regulated Peltier cooling. (3) A sufficiently low light level at the photocathodes and a sufficiently low average anode current. Light intensities were measured with the photon-counting technique.

Choppers

For the discrimination between prompt and delayed fluorescence, a double chopper with 40 slits and a rotation frequency of ≈ 500 Hz was used (cf. Fig. 4 in [22]). The resulting chop frequency was ≈ 20 kHz. For the measurement of the time dependence of the delayed fluorescence, the excitation light beam was

additionally chopped with a slow chopper with one slit and a chop frequency of 50 Hz. The slow chopper was located between the argon ion laser and the fast chopper. The measurement of the time dependence of the delayed fluorescence was triggered by the slow chopper. By this combination of two unsynchronized choppers it was possible to measure not only the decay but also the rise of the delayed fluorescence.

3. Experimental Results

3.1 Absorption spectrum and spectra of prompt and delayed fluorescence

The absorption spectrum at 298 K and the prompt-fluorescence spectrum at 153 K of fluoroanthene in 3-methylpentane are shown in Fig. 1. The prompt fluorescence was excited with the UV lines of an argon ion laser at 333.6 and 334.5 nm, whose Rayleigh scattering was observed in first diffraction order at $\approx 30\,000\text{ cm}^{-1}$ and in second diffraction order at $\approx 15\,000\text{ cm}^{-1}$. The narrow band at $\approx 27\,000\text{ cm}^{-1}$ is Raman-scattered light mainly due to the C–H stretching modes of 3-methylpentane.

The contributions of DEF and DMF to the total delayed fluorescence are shown in Fig. 2 for three temperatures. The difference spectrum between the

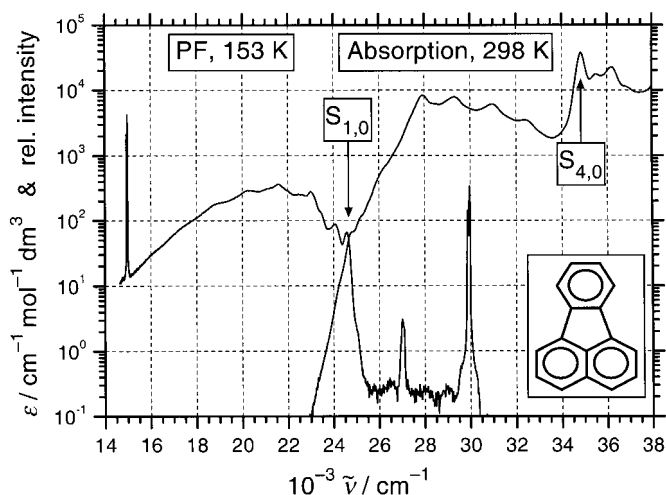


Fig. 1. Absorption spectrum at 298 K and prompt-fluorescence spectrum at 153 K of fluoroanthene in 3-methylpentane. The prompt fluorescence was excited with the UV lines of an argon ion laser at 333.6 and 334.5 nm, whose Rayleigh scattering was observed in first diffraction order at $\approx 30\,000\text{ cm}^{-1}$ and in second diffraction order at $\approx 15\,000\text{ cm}^{-1}$. The narrow band at $\approx 27\,000\text{ cm}^{-1}$ is Raman scattered light mainly due to the C–H stretching modes of 3-methylpentane.

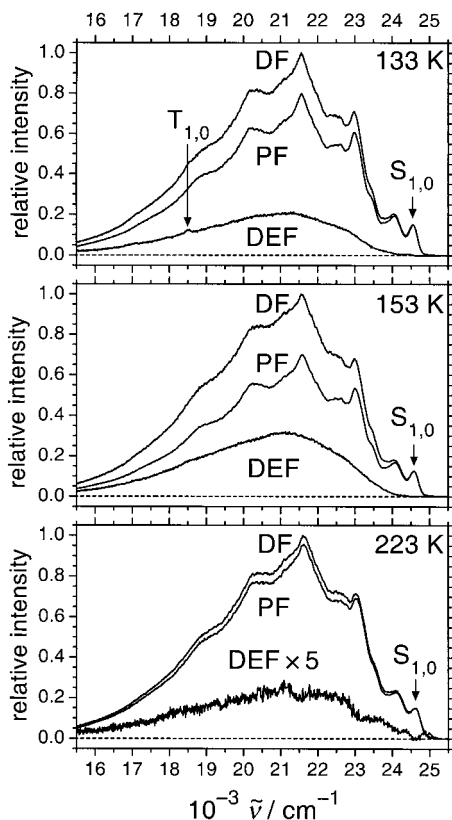


Fig. 2. Spectra of the total delayed fluorescence (DF), the prompt fluorescence (PF), and the delayed excimer fluorescence (DEF) of fluoranthene ($2 \cdot 10^{-5}$ mol dm $^{-3}$) in 3-methylpentane at three temperatures. The contribution of the phosphorescence (0-0 transition at 18500 cm $^{-1}$) to the total long-lived emission was always very small.

spectrum of the total long-lived luminescence and the spectrum of the prompt fluorescence contains also the phosphorescence spectrum, which should be subtracted from the difference spectrum. At the lowest temperature (133 K) the 0-0 transition of the phosphorescence at 18500 cm $^{-1}$ is discernible. In principle, the pure phosphorescence spectrum can be determined as difference spectrum of delayed-luminescence spectra measured with different excitation intensities (cf. e.g. [23,24]). In practice a phosphorescence correction was dispensable, because the resulting absolute change of the intensity ratio Q_{EM} of DEF and DMF was always smaller than the absolute accuracy of ± 0.02 of Q_{EM} .

The DEF spectrum for 223 K in Fig. 2 illustrates a problem in the determination of Q_{EM} . The DEF spectrum has indentations at the wavenumbers of

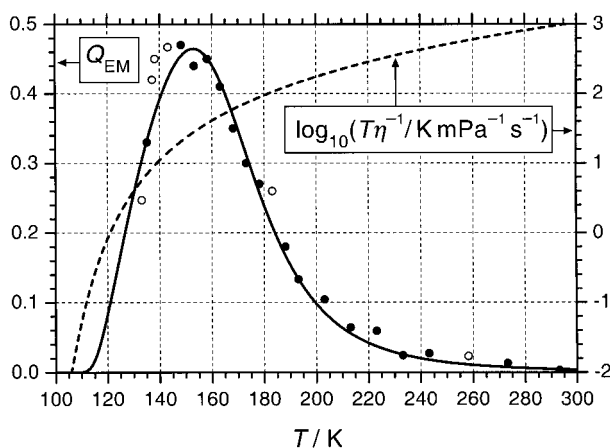


Fig. 3. Intensity ratio $Q_{EM}(T)$ of DEF and DMF. The solid line is a theoretical curve, which was obtained by fitting a kinetic model (cf. Sects. 4 and 5) to the data points that are represented by full circles. The theoretical curve is identical with the solid curve in Fig. 10a. The viscosity η was calculated with Eq. (3-1).

the maxima in the PF spectrum between 21 000 and 25 000 cm^{-1} . These indentations could be removed by reducing the normalization factor of the PF spectrum by 5 to 10%, but the resulting difference spectrum would have a far too high intensity at 24 600 cm^{-1} . Therefore the present difference spectrum is preferred. The residual structure in the difference spectrum for 223 K can be caused by an imperfect correction for intensity fluctuations. The data for 153 K represent the highest quality achieved, and the data for 223 K represent the lowest acceptable quality.

The temperature dependence of Q_{EM} is shown in Fig. 3. Apart from the experimental values of Q_{EM} , a theoretical curve for Q_{EM} (cf. Sects. 4 and 5) and the logarithm of the ratio T/η of the temperature T and the viscosity η of 3-methylpentane are also shown in Fig. 3. The temperature dependence of the viscosity was calculated with the empirical equation

$$\eta = A_1 \exp(T_1/T) + A_2 \exp(T_2/T) + A_3 \exp[T_3/(T - T_0)] \quad (3-1)$$

with $A_1 = 1.950 \cdot 10^{-2}$ mPa s, $T_1 = 802.38$ K, $A_2 = 1.996 \cdot 10^{-6}$ mPa s, $T_2 = 2087.86$ K, $A_3 = 5.422 \cdot 10^{-7}$ mPa s, $T_3 = 1187.53$ K, $T_0 = 55.718$ K [25].

3.2 Time dependence of delayed fluorescence

If the observed delayed luminescence between 19 000 and 25 000 cm^{-1} is exclusively due to TTA of fluoranthene, then the time dependence of the delayed luminescence in that spectral range must be independent of the observation

wavelength. This expectation was confirmed by measuring the time dependence of the delayed luminescence at 406 nm (0-0 transition of the delayed monomer fluorescence) and at 457 nm (close to the maxima of DMF and DEF). The temperature was 153 K (maximum of $Q_{EM}(T)$). The time dependence of I_{DF} for the two wavelengths is shown in Fig. 4a. The ratio I_{406}/I_{457} in Fig. 4b exhibits no significant deviation from a constant value.

The kinetic consistency of the rise and the initial decay of the delayed fluorescence at 457 nm is demonstrated as follows. Let a sample be excited with constant intensity in the time interval (t_0, t_1) . If ground-state depletion and TTA as triplet decay process are completely neglected, then the triplet concentration in the time interval (t_0, t_1) is given by

$$c_T(t) = (c_T)_{\max}[1 - \exp(-k_T(t - t_0))], \quad (3-2)$$

where k_T is the first-order rate constant for the triplet decay. The corresponding intensity of the delayed fluorescence during the rise of the triplet concentration is

$$(I_{DF})_{\text{rise}} = C[(c_T)_{\max}]^2 [1 - 2 \exp(-k_T(t - t_0)) + \exp(-2k_T(t - t_0))], \quad (3-3)$$

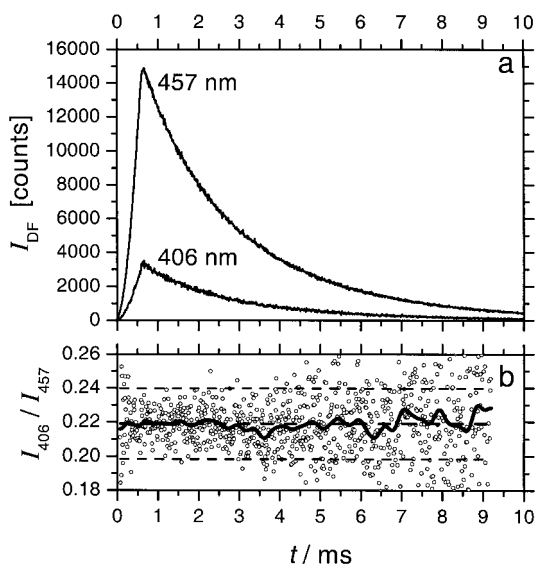


Fig. 4. (a) Rise and decay of the delayed fluorescence at the 0-0 transition of the delayed monomer fluorescence (406 nm) and at the maximum of the DF spectrum (457 nm). (b) Ratio of the two curves. The thick solid curve was obtained by strong smoothing of the original data.

where C is an experimental constant. The subsequent decay of the delayed fluorescence is given by

$$(I_{\text{DF}})_{\text{decay}} = C[c_{\text{T}}(t_1)]^2 \exp[-2k_{\text{T}}(t - t_1)]. \quad (3-4)$$

An effective triplet decay rate constant $k_{\text{T}} = (227.5 \pm 1.3) \text{ s}^{-1}$ was obtained by fitting the exponential function (3-4) to the decay of I_{DF} between 0.66 and 2.00 ms (right solid curve) in Fig. 5. Eq. (3-3) was fitted to the rise of I_{DF} between 0.02 and 0.55 ms by using the same value of k_{T} and treating t_0 and the amplitude factor $C[(c_{\text{T}})_{\text{max}}]^2$ as adjustable parameters. The fitted value $t_0 = (-0.046 \pm 0.001) \text{ ms}$ is consistent with the fact that the measurement of the delayed fluorescence was triggered by the laser beam passing the slow chopper (cf. the item *choppers* in Sect. 2). The inverse edge velocity of the chopper blade of the slow chopper was $\approx 35 \mu\text{s}/\text{mm}$. Thus t_0 is of the order of magnitude of the time needed by the edge of the chopper blade for crossing a laser beam of about 2 mm diameter.

The fitted rise and decay curves intersect at $t_1 = (0.600 \pm 0.001) \text{ ms}$. The significant deviation of the two fitted curves from the experimental values at the time t_1 is caused in part by the finite time needed by the slow chopper blade for crossing the laser beam and in part by the finite chop frequency of the fast

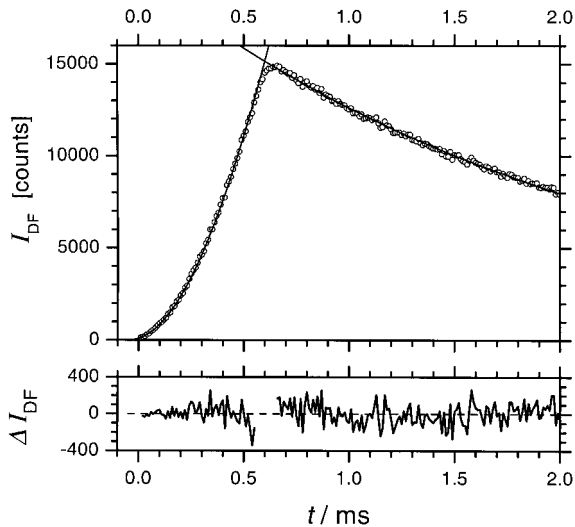


Fig. 5. Kinetic consistency of the rise and the initial decay of the delayed fluorescence at 457 nm. An effective triplet decay rate constant $k_{\text{T}} = (227.5 \pm 1.3) \text{ s}^{-1}$ was obtained by fitting Eq. (3-4) to the decay of I_{DF} between 0.66 and 2.0 ms (right solid curve). The left solid curve was obtained by fitting Eq. (3-3) to the rise of the delayed fluorescence, with the same value of k_{T} and with t_0 and the amplitude factor as adjustable parameters. ΔI_{DF} is the difference between the experimental curves and the fitted theoretical curves.

chopper (20 kHz). In principle, both causes can be taken into account in a more sophisticated description of the time dependence of the delayed fluorescence. Nevertheless, even the present simple description of the time dependence of the delayed fluorescence permits the conclusion that there is no indication of a more complex kinetic behavior, such as triplet-triplet energy transfer to impurities and a contribution of impurities to the observable delayed fluorescence. The deviation of the decay of the delayed fluorescence from a strictly monoexponential decay is caused by a nonnegligible initial contribution of TTA to the total triplet decay.

The spectra of the delayed fluorescence were measured with a much higher average triplet concentration, at which TTA was already the dominant triplet decay process. Due to the corresponding shortening of the average triplet lifetime, the conceivable contribution of a sensitized delayed impurity fluorescence to the total delayed fluorescence was smaller than in the case of the kinetic measurements.

4. Kinetic model

The kinetic model consists of two parts. The first part describes the generation of ${}^1M^* \cdots {}^1M$ pairs by triplet-triplet annihilation. The second part describes the subsequent evolution of the ${}^1M^* \cdots {}^1M$ pair distribution function, from which the observable ratio of the intensities of delayed excimer fluorescence and delayed monomer fluorescence can be calculated.

4.1 Generation of ${}^1M^* \cdots {}^1M$ pairs by triplet-triplet annihilation

The kinetic treatment of the generation of ${}^1M^* \cdots {}^1M$ pairs by triplet-triplet annihilation is similar to that applied by Butler and Pilling [21]. The only essential difference will be a distance-dependent relative diffusion coefficient $D = D(r)$. Let $\rho_T(r, t)$ be the relative probability density of finding triplet molecules at the distance r from the center of a selected triplet molecule; ρ_T is normalized to $\rho_T(\infty, t) = 1$. The evolution of the distribution function ρ_T is governed by the partial differential equation

$$\frac{\partial \rho_T(r, t)}{\partial t} = \frac{1}{r^2} \frac{\partial}{\partial r} \left(r^2 D(r) \frac{\partial \rho_T(r, t)}{\partial r} \right) - k_{1A}(r) \rho_T(r, t). \quad (4-1)$$

k_{1A} is the distance-dependent first-order rate coefficient for the annihilation of a triplet pair. In principle Eq. (4-1) is to be solved for the adequate initial condition $\rho_T(r, 0)$ and adequate boundary conditions. In previous papers [26, 27] it was shown that the initial condition for TTA strongly differs from the Smoluchowski initial condition $\rho_T(r, 0) = 1$ for $r \geq R_0$, where R_0 is the contact distance of hard spheres. The different initial condition leads to an anomalous initial time dependence of the delayed fluorescence in viscous solution, if the

delayed fluorescence is measured with a short dead time after pulsed excitation of a sample. In the present study, the viscosity was low or moderately large at most and the excitation was quasi-continuous. Thus ρ_T was in good approximation equal to the steady-state distribution $\rho_T(r) \equiv \rho_T(r, \infty)$. In the steady state with $\partial\rho/\partial t = 0$, the partial differential Eq. (4-1) reduces to the ordinary differential equation

$$\frac{1}{r^2} \frac{d}{dr} \left(r^2 D(r) \frac{d\rho_T(r)}{dr} \right) - k_{1A}(r) \rho_T(r) = 0, \quad (4-2)$$

which is numerically solved with the inner boundary condition

$$\left(\frac{d\rho_T(r)}{dr} \right)_{r=R_0} = 0. \quad (4-3)$$

Eq. (4-3) means that the molecular contact involves no additional contribution to TTA.

The relative probability density for the transformation of a triplet pair ${}^3M^* \dots {}^3M^*$ with the intermolecular distance r into a singlet pair ${}^1M^* \dots {}^1M$ is

$$\rho_S(r, 0) = C k_{1A}(r) \rho_T(r), \quad (4-4)$$

where C is a normalization factor corresponding to

$$4\pi \int_{R_0}^{\infty} \rho_S(r, 0) r^2 dr = 1. \quad (4-5)$$

Two different annihilation radii are of interest. The mean annihilation radius R_{TTA} is defined by

$$R_{TTA} = 4\pi \int_{R_0}^{\infty} \rho_S(r, 0) r^3 dr. \quad (4-6)$$

An effective annihilation radius R_{eff} can be calculated by defining the second-order rate constant for TTA,

$$k_{2A} = 4\pi D(\infty) R_{\text{eff}}, \quad (4-7)$$

according to Smoluchowski's theory [28–30] and by taking into account that, outside the radial near zone, where annihilation takes place and $D = D(r)$, $\rho_T(r)$ must be equal to Smoluchowski's formula for the steady-state solution:

$$\rho_{\text{Smol}}(r, \infty) = 1 - \frac{R_{\text{eff}}}{r}. \quad (4-8)$$

Note that always $R_{TTA} > R_0$, whereas R_{eff} can be smaller than R_0 .

4.2 Evolution of the ${}^1\text{M}^* \dots {}^1\text{M}$ pair distribution function

The relative diffusive motion of the two molecules in an ${}^1\text{M}^* \dots {}^1\text{M}$ pair is restricted to the radial range $R_0 \leq r \leq R_N$. The outer reflecting boundary R_N is defined by the requirement that the volume $V(R_0, R_N)$ of the spherical shell between R_0 and R_N be equal to the volume per solute molecule in the solution,

$$V(R_0, R_N) = (4\pi/3)(R_N^3 - R_0^3) = (c_0 N_A)^{-1}, \quad (4-9)$$

where c_0 is the molar concentration of the solute and N_A is the Avogadro number. By this restriction, the non-geminate formation of an excimer is approximately taken into account. In the present case with $c_0 \approx 2 \cdot 10^{-5} \text{ mol dm}^{-3}$ one obtains $R_N \approx (4\pi c_0 N_A/3)^{-1/3} \approx 2.7 \cdot 10^{-7} \text{ dm} = 27 \text{ nm}$.

An excimer is represented by a short-range attractive potential $U(r)$ with the halfwidth Γ . The radial range $R_0 \leq r \leq R_0 + \Gamma$ is assigned to the excimer, and the radial range $R_0 + \Gamma < r \leq R_N$ to the excited monomer. $U(r)$ has to satisfy the boundary condition

$$\left(\frac{dU(r)}{dr} \right)_{r=R_0} = 0. \quad (4-10)$$

The rate coefficient k_S for the total (radiative and nonradiative) decay of an ${}^1\text{M}^* \dots {}^1\text{M}$ pair depends on the distance r , $k_S = k_S(r)$. The resulting Smoluchowski equation [29–31] for the evolution of ρ_S is

$$\frac{\partial \rho_S(r, t)}{\partial t} = \frac{1}{r^2} \frac{\partial}{\partial r} \left(r^2 D(r) \left[\frac{\partial \rho_S(r, t)}{\partial r} + \frac{1}{k_B T} \frac{dU(r)}{dr} \rho_S(r, t) \right] \right) - k_S(r) \rho_S(r, t), \quad (4-11)$$

where k_B is the Boltzmann constant and T is the temperature. Eq. (4-11) is to be solved for the inner boundary condition

$$\left(\frac{\partial \rho_S(r, t)}{\partial r} \right)_{r=R_0} = 0. \quad (4-12)$$

and the outer boundary condition

$$\left(\frac{\partial \rho_S(r, t)}{\partial r} \right)_{r=R_N} = 0. \quad (4-13)$$

The probabilities for the existence of an excimer, $p_E(t)$, and an excited monomer, $p_M(t)$, are defined by

$$p_E(0) + p_M(0) = 1 \quad (4-14)$$

$$p_E(t) = 4\pi \int_{R_0}^{R_0+\Gamma} \rho_S(r, t) r^2 dr \quad (4-15)$$

$$p_M(t) = 4\pi \int_{R_0+\Gamma}^{R_N} \rho_S(r, t) r^2 dr . \quad (4-16)$$

The experimentally accessible quantity is the ratio of the spectrally integrated intensities of delayed excimer fluorescence and delayed monomer fluorescence:

$$Q_{EM} = \frac{I_{DEF}}{I_{DMF}} = \frac{k_E^{\text{rad}} \int_0^\infty p_E(t) dt}{k_M^{\text{rad}} \int_0^\infty p_M(t) dt} , \quad (4-17)$$

where k_E^{rad} and k_M^{rad} are the rate constants for the radiative decay of the excimer and the excited monomer. In practice, an upper integration limit $t_\infty \approx 10/(k_S)_{\text{min}}$ will be virtually equivalent to infinity.

Finally, the mean radii R_E for DEF and R_M for DMF can be calculated as follows. First, for each discrete time t the corresponding mean radii $R_E(t)$ and $R_M(t)$ are calculated,

$$R_E(t) = \left[4\pi \int_{R_0}^{R_0+\Gamma} \rho_S(r, t) r^3 dr \right] / p_E(t) , \quad (4-18)$$

with an analogous expression for $R_M(t)$. Second, the averages of $R_E(t)$ and $R_M(t)$ with respect to the time t are calculated:

$$R_E = \left(\int_0^\infty R_E(t) p_E(t) dt \right) / \left(\int_0^\infty p_E(t) dt \right) , \quad (4-19)$$

and an analogous expression for R_M .

5. Application of the kinetic model

In the actual application of the kinetic model to the experimental data in Fig. 3 one meets three principal difficulties. First, since the fluoranthene molecule is not even approximately spherical, the contact radius R_0 and all distance-dependent quantities will depend on the relative orientation of

two interacting solute molecules. Hence the choice of a contact radius R_0 will be arbitrary to some degree. Second, the radial dependences $D = D(r)$, $k_{1A} = k_{1A}(r)$, $U = U(r)$, and $k_S = k_S(r)$ are unknown. Third, even if the kinetic model were exact and if the accuracy of the experimental values of $Q_{EM}(T)$ in Fig. 3 were much higher, it would be nevertheless impossible to determine eight or more parameter values by fitting the kinetic model to the experimental data.

5.1 Molecular diameters and relative diffusion coefficient

In general, in the case of nonspherical molecules, the effective molecular diameter R_{av} is assumed to be equal to the diameter of a sphere, whose volume is equal to the van-der-Waals volume of the nonspherical molecule. For fluoranthene $R_{av} \approx 0.75$ nm is obtained. On the other hand, the distance between the planes of the two molecules in a sandwich excimer is ≈ 0.35 nm [4]. We take the latter radius as contact radius R_0 .

The relative Brownian motion of the two molecules in a sandwich pair must be strongly correlated. With respect to the kinetic model that means, $D(R_0)$ must be much smaller than $D(\infty)$. In our arbitrary choice of $D(r)$ we start from the simple expression proposed by Northrup and Hynes [32],

$$D(r) = D(\infty) [1 - a_{dif} \exp(-(r - R_{av})/R_{av})] , \quad (5-1)$$

where $a_{dif} = 0.5$. We assume that Eq. (5-1) can be used also in the range $R_0 \leq r < R_{av}$ as long as $D(R_0) > 0$ and write Eq. (5-1) in a slightly different form:

$$D(r) = D(\infty) [1 - b_{dif} \exp(-(r - R_0)/R_{av})] , \quad (5-2)$$

where

$$b_{dif} = a_{dif} \exp [(R_{av} - R_0)/R_{av}] . \quad (5-3)$$

With $R_{av} = 0.75$ nm, $R_0 = 0.35$ nm, and $a_{dif} = 0.5$ one obtains $b_{dif} \approx 0.85$. The numerical results in Sect. 5.4 were obtained with $b_{dif} = 0.85$. Finally we assume an identical distance dependence for the relative diffusion coefficient of two molecules in the triplet state.

The absolute value of $D(\infty) = 2D_0$ was obtained by assuming an equality of the diffusion coefficients of fluoranthene and pyrene and the proportionality $D_0 \propto T/\eta$ according to the Stokes-Einstein equation. The measured value of the diffusion coefficient of ³pyrene* in hexane at 298.16 K is $D_0 = 2.93 \cdot 10^9 \text{ nm}^3 \text{ s}^{-1}$ [33] ($\eta_{\text{hexane}}(293.16 \text{ K}) = 0.2985 \text{ mPa s}$).

5.2 Radial dependence of k_{1A}

A simple radial dependence of the rate coefficient k_{1A} for the annihilation of a triplet pair can be expected only for large distances r , e.g. $r \geq 2R_{av}$, where $k_{1A}(r)$ is smaller than the rate constant for orientational relaxation and details of the molecular shape no longer matter. In this case, the exponential distance dependence, which is usually assumed for processes depending on exchange interaction, is probably a good approximation [21],

$$k_{1A} = A \exp(-2r/L) = k_{1A}(R_0) \exp(-2(r - R_0)/L), \quad (5-4)$$

where A is a frequency factor and L is a characteristic length. We assume that Eq. (5-4) is the best two-parameter approximation to $k_{1A}(r)$ also in the near zone $R_0 \leq r \leq 2R_{av}$.

5.3 Effective excimer potential

The effective excimer potential $U(r)$ must satisfy two general requirements. First, in combination with the hard-sphere approximation, relative diffusion is restricted to $r \geq R_0$, which entails $U'(R_0) = 0$, where $U'(r) \equiv dU(r)/dr$. Second, the effective range of the potential must be small. We use the most simple two-parameter potential

$$U(r) = U(R_0) \exp(-\ln(2) [(r - R_E)/\Gamma]^{2\kappa}). \quad (5-5)$$

with $\kappa \geq 1$. For high powers of κ this potential becomes a good approximation to a box potential. The radial range $R_0 \leq r \leq R_0 + \Gamma$ is assigned to the excimer.

The choice of the radial dependence of the decay rate constant $k_S = k_S(r)$ is not critical in the case of fluoranthene, as will be shown below.

5.4 Choice of fixed parameters

In the application of the kinetic model to the experimental data in Fig. 3 it turns out that it is impossible to determine more than three free parameters. The number of free parameters or their ranges of acceptable values are reduced as follows:

(a) The rate constant k_M for the decay of the excited monomer is known [12] and independent of temperature [34]. The rate constant k_M^{rad} [35] for the radiative decay of the excited monomer is also assumed to be independent of temperature.

(b) The rate constants for the total decay and the radiative decay of the excimer to the ground-state dimer are assumed to be equal to the corresponding rate constants for the monomer: $k_E = k_M$ and $k_E^{\text{rad}} = k_M^{\text{rad}}$. This assumption is justified on the one hand by the reported concentration independence of the

quantum yield and the lifetime of the fluorescence from solutions of fluoranthene [12, 13] and on the other hand by the measured fluorescence lifetime of 55 ns of solid amorphous films of fluoranthene at low temperatures [36] (the latter fluorescence was assigned by the authors of [36] to the excimer of fluoranthene).

(c) Experimental steady-state values of the second-order rate coefficient k_{TTA} for TTA in low-viscosity solvents are significantly smaller than the theoretical value calculated with Smoluchowski's steady-state expression $k_2 = 4\pi D(\infty)R_{\text{av}}$ for a diffusion-controlled reaction of the type $A + A \rightarrow C$ [37–39]. E.g., for anthracene and pyrene in cyclohexane at room temperature, $(k_2)_{\text{expt}} \approx 0.25(k_2)_{\text{Smol}}$ [39]. In part this discrepancy results from the fact that Smoluchowski's expression implies the removal of two particles A by one encounter, whereas the annihilation of two triplet states entails the disappearance of less than two triplet states on the average. On the one hand, in the dominant triplet channel of TTA [38], $T_1 + T_1 \rightarrow S_0 + T_m$, the primarily produced upper triplet state T_m relaxes to T_1 ; on the other hand, in the singlet channel of TTA, part of the molecules in S_1 also relax to T_1 due to intersystem crossing. Thus, on the average only a little more than one T_1 is removed by the reactive encounter of two T_1 . In the following, an effective radius R_{eff} of TTA, $R_{\text{eff}} \approx R_{\text{av}}/2$ is postulated for the temperature $T_{3\text{MP}}$, at which the diffusion coefficient D_0 of $^3\text{fluoranthene}^*$ in 3-methylpentane (3MP) equals the diffusion coefficient of $^3\text{pyrene}^*$ in cyclohexane (CH) at $T_{\text{CH}} \approx 298$ K. With $T_{3\text{MP}}/\eta_{3\text{MP}} = T_{\text{CH}}/\eta_{\text{CH}}$ and $\eta_{\text{CH}}(298 \text{ K}) = 0.898 \text{ mPa s}$ and the known temperature dependence of $\eta_{3\text{MP}}$ one obtains $T_{3\text{MP}} \approx 227$ K. The temperature of the closest experimental point is 223 K. Thus we postulate $R_{\text{eff}}(223 \text{ K}) = 0.4 \text{ nm} \approx R_{\text{av}}/2$.

The remaining free parameters are $U(R_0)$, Γ , κ , L , $k_{1A}(R_0)$. The numerical calculations were performed with $\kappa = 1, 2, 3$.

5.5 Computational aspects

The accurate numerical solution of the ordinary differential equation (4-2) offers no difficulties. The accurate numerical solution of the partial differential equation (4-11) is less trivial because of the required long diffusion time of the order of 500 ns. A new algorithm [40] was employed, whose distinctive feature is the systematic use of numerical fundamental solutions. By expressing the fundamental solutions at the time $2t$ as linear combinations of the fundamental solutions at the time t , successive doubling of the total diffusion time becomes possible up to the total diffusion time $4 \text{ ns} \approx 0.1/k_S$; for longer times, constant time steps of 4 ns were used up to $532 \text{ ns} \approx 10/k_S$ (for details cf. [40]). The power κ and the halfwidth Γ in the potential (Eq. (5-5)) were fixed. The depth of the potential, $U(R_0)$, the frequency factor $k_{1A}(R_0)$ and the length L (cf. Eq. (5-4)) were treated as adjustable parameters, whose best values were obtained by a Simplex least-squares method [41]. The fit criterion was the agreement of the theoretical curve $Q_{\text{EM}}(T)$ with the experimental

values of Q_{EM} . By a variation of Γ , different values of the effective annihilation radius R_{eff} (223 K) were obtained. The values of Γ corresponding to the selected values 0.35 nm, 0.40 nm and 0.45 nm of R_{eff} (223 K) were obtained by quadratic interpolation. With $\kappa = 1$, the value $R_{eff} = 0.35$ nm cannot be reached (R_{eff} (223 K, Γ) has a minimum > 0.35 nm). In order to obtain a good description of $Q_{EM}(T)$ in the temperature range between 150 and 293 K, not all experimental values of Q_{EM} were used in the fit procedure.

5.6 Numerical results

The basic steps in the computation of the intensity ratio Q_{EM} of DEF and DMF are illustrated by Figs. 6 to 8. The numerical solution of Eq. (4-2) is shown in Fig. 6 for $\kappa = 2$, R_{eff} (223 K) = 0.40 nm, and the temperature 223 K. The curve $\rho_T(r)$ asymptotically approaches the Smoluchowski steady-state distribution $\rho_{Smol}(r)$ at distances, where the radial dependence of the relative diffusion coefficient disappears. The normalized initial radial singlet probability distribution $4\pi r^2 \rho_S(r, 0)$ and the radial dependences of the first-order TTA rate coefficient k_{1A} and of the excimer potential U are also shown.

The evolution of the radial probability density $4\pi r^2 \rho_S(r, t) \exp(+k_S t)$ at 223 K is shown in Fig. 7 in a double-logarithmic plot. Curve 13 ($t = 256$ ns) illustrates a peculiarity of the numerical algorithm. The mean radii of successive spherical shells increase by an almost constant factor $f_1 = 1 + q_1$ in the range of the potential and by an also almost constant factor $f_2 = 1 + q_2$ at large

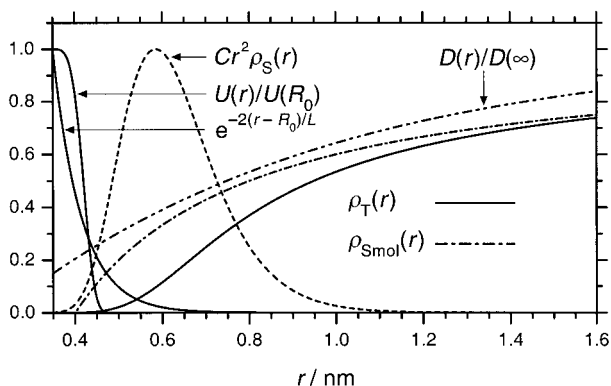


Fig. 6. Steady-state ${}^3M^* \dots {}^3M^*$ distribution $\rho_T(r)$ (—), Smoluchowski steady-state distribution $\rho_{Smol}(r)$ (---), and initial radial probability density of ${}^1M^* \dots {}^1M$ distribution, $Cr^2 \rho_S(r)$ (· · · · ·) at 223 K; radial dependences of the relative diffusion coefficient, $D(r)/D(\infty)$ (— · — · —) (Eq. (5-2) with $b_{dif} = 0.85$), of the first-order rate coefficient for TTA, $k_{1A}(r)/k_{1A}(R_0) = \exp(-2(r - R_0)/L)$, and of the relative excimer potential $U(r)/U(R_0)$. All curves are normalized to a maximum of unity. Parameters: See Table 1, R_{eff} (223 K) = 0.400 nm, $\kappa = 2$.

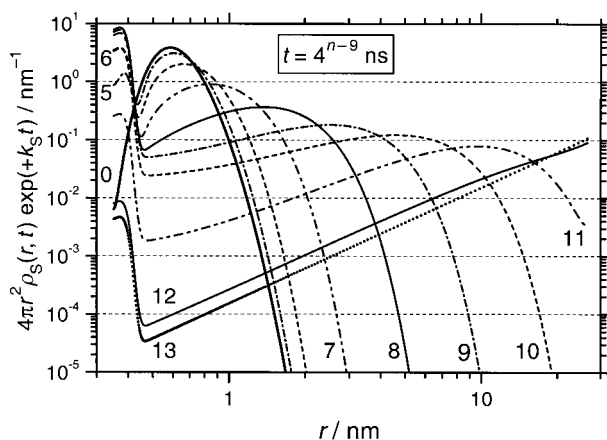


Fig. 7. Evolution of the radial singlet probability density without excited-state decay, $4\pi r^2 \rho_S(r, t) \exp(+k_S t)$, at 223 K (same parameters as in Fig. 6). The labels 0, 5, 6, ... are equal to n in the exponent of $t = 4^{n-9}$ ns.

radii, with a smooth transition from q_1 to q_2 . Curve 13 already coincides with the equilibrium distribution.

For each discrete time t the excimer probability $p_E(t)$ is computed from $\rho_S(r, t)$ according to Eq. (4-15). In Fig. 8, $p_{E0}(t) \equiv p_E(t) \exp(+k_S t)$ is shown in a double-logarithmic plot for different temperatures. The curve for 298 K illustrates the successive time-doubling up to the total diffusion time of 4 ns and the subsequent constant time step of 4 ns up to final diffusion time of 532 ns $\approx 10/k_S$. For the numerical integration of $p_E(t)$ and the analogous $p_M(t)$, the discrete points were interpolated with a cubic spline [41].

For the later discussion of the observability of prompt excimer fluorescence, an effective first-order rate constant k_{diss} for the dissociation of the excimer will be of interest. k_{diss} can be defined as follows. A semilogarithmic plot of $p_{E0}(t)$ reveals that $\ln p_{E0}(t)$ has an inflection point in the range $0.35 \geq p_{E0} \geq 0.2$ and is approximately linear within an order of magnitude or more, i.e. in the time range, where most of the dissociation takes place. k_{diss} was defined by the slope of $p_{E0}(t)$ at the inflection point. $k_{\text{diss}}(T)$ was calculated from 298 to 150 K in steps of 4 K with the three sets of parameters belonging to $R_{\text{eff}} = 0.40$ nm (cf. Table 1). In the Arrhenius plot of Fig. 9, the deviations of $\log_{10}(k_{\text{diss}}/\text{s}^{-1})$ from straight lines are significant only below 200 K. An activation energy for excimer dissociation, $E_a(k_{\text{diss}})$, was determined by fitting the exponential function $\exp(-E_a(k_{\text{diss}})/k_B T)$ to $k_{\text{diss}}(T)$ between 298 and 202 K. $E_a(k_{\text{diss}})$ is approximately equal to the sum of the activation energy of T/η (i.e. of the relative diffusion coefficient) and of the binding enthalpy of the excimer, B_E , which is obtained from the temperature dependence of the excimer-monomer equilibrium constant $K_{\text{EM}}^{(1)} = (p_E^{(1)}/p_M^{(1)})_{\text{eq}}$ (the superscript ⁽¹⁾ indicates that the excimer-monomer equilibrium refers to a single

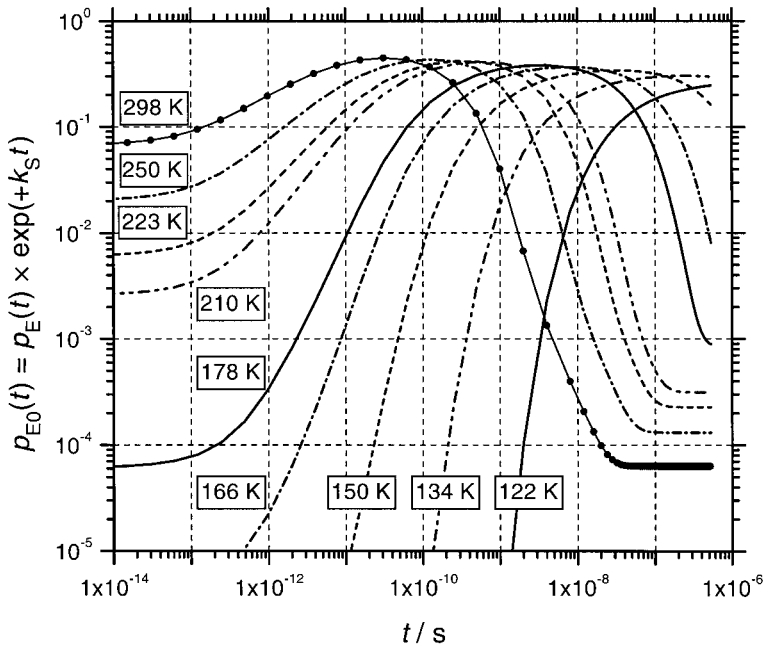


Fig. 8. Time dependence of the relative excimer probability without excited-state decay, $p_{E0}(t) = p_E(t) \exp(+k_S t)$, at different temperatures (same parameters as in Fig. 6).

Table 1. Parameter combinations for all theoretical curves in the paper. R_{eff} is the effective Smoluchowski radius for TTA at 223 K according to Eq. (4-8). κ , Γ and $U(R_0)/hc$ define the excimer potential in Eq. (5-5). $L/2$ and $k_{1A}(R_0)$ define the exponential distance dependence of TTA in Eq. (5-4).

R_{eff} [nm]	κ	Γ [nm]	$U(R_0)/hc$ [cm ⁻¹]	$L/2$ [nm]	$k_{1A}(R_0)$ [s ⁻¹]
0.3498	2	0.04282	-896	0.05525	$3.144 \cdot 10^{12}$
0.3502	3	0.05373	-843	0.05927	$2.220 \cdot 10^{12}$
0.4000	1	0.03814	-989	0.05185	$1.117 \cdot 10^{13}$
0.4000	2	0.06979	-843	0.06425	$3.174 \cdot 10^{12}$
0.4005	3	0.08244	-797	0.06745	$2.430 \cdot 10^{12}$
0.4500	1	0.05624	-950	0.059055	$1.168 \cdot 10^{13}$
0.4500	2	0.09312	-815	0.07025	$3.845 \cdot 10^{12}$
0.4501	3	0.10821	-770	0.07342	$2.956 \cdot 10^{12}$

ground-state molecule in the finite volume V). The temperature dependences of T/η , $k_{\text{diss}}\eta T^{-1}$ and $K_{\text{ME}}^{(1)} \equiv (K_{\text{EM}}^{(1)})^{-1}$ are also shown in Fig. 9, and the values of $E_a(k_{\text{diss}})$, $E_a(T/\eta)$, and B_E are listed in Table 2.

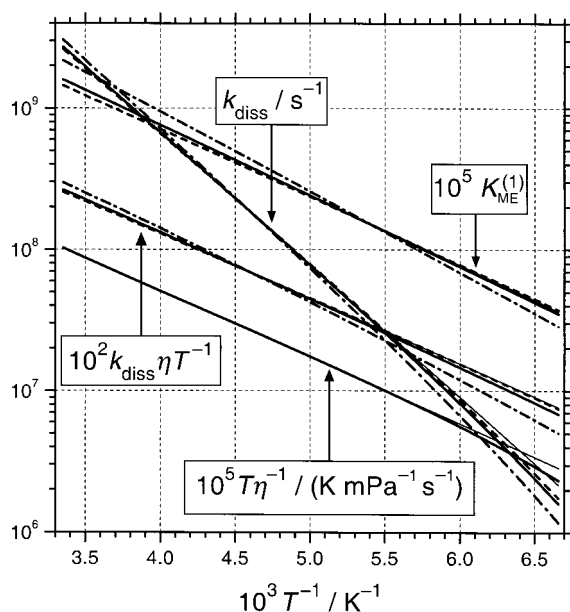


Fig. 9. Temperature dependence of the first-order rate constant of excimer dissociation, k_{diss} , the monomer-excimer equilibrium constant $K_{\text{ME}}^{(1)} \equiv (K_{\text{EM}}^{(1)})^{-1}$, and of the ratio T/η . The computations were performed with $R_{\text{eff}} = 0.400$ nm and $\kappa = 1$ (---), $\kappa = 2$ (—), $\kappa = 3$ (- - -) cf. Table 1). The corresponding activation energies and the excimer binding enthalpy in Table 2 were obtained by fitting exponentials to the curves in the temperature range between 298 K and 202 K; the fitted exponentials are shown for $\kappa = 2$ as thin solid lines.

Table 2. Activation energies E_a and excimer binding enthalpy B_E , derived from the temperature dependence of k_{diss} , T/η , $k_{\text{diss}}\eta T^{-1}$ and $K_{\text{EM}}^{(1)}$ between 202 and 293 K (cf. Fig. 9). All values refer to $R_{\text{eff}}(223 \text{ K}) = 0.400$ nm. For comparison the respective values of the potential minimum, $U(R_0)$, are also given.

κ	$E_a(k_{\text{diss}})/hc$ [cm ⁻¹]	$E_a(T/\eta)/hc$ [cm ⁻¹]	$E_a(k_{\text{diss}}\eta T^{-1})/hc$ [cm ⁻¹]	B_E/hc [cm ⁻¹]	$U(R_0)/hc$ [cm ⁻¹]
1	1557	752	808	-895	-989
2	1498	752	745	-794	-843
3	1481	752	727	-763	-797

The main final results of the kinetic model are presented in Fig. 10 as functions of the reciprocal temperature. Eight theoretical curves $Q_{\text{EM}}(T)$ were calculated – see Table 1. Of the eight curves, three are compared with the experimental data in Fig. 10a. The solid curve ($\kappa = 2$, $R_{\text{eff}} = 0.40$ nm) is identical with the solid curve in Fig. 3. The two other theoretical curves are those with

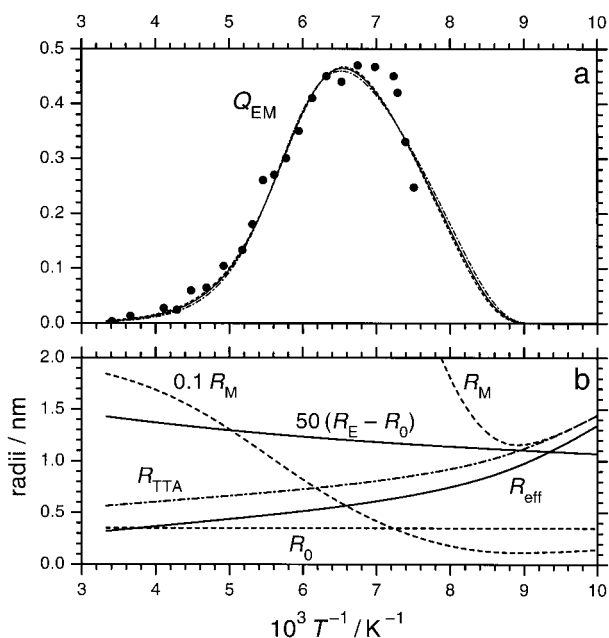


Fig. 10. (a) Intensity ratio $Q_{EM}(T)$ of DEF and DMF. Experimental values $\bullet\bullet\bullet$; the three theoretical curves were computed with $R_{eff}(223\text{ K}) = 0.400\text{ nm}$, $\kappa = 2$ (—), $R_{eff}(223\text{ K}) = 0.400\text{ nm}$, $\kappa = 1$ (---), and $R_{eff}(223\text{ K}) = 0.45\text{ nm}$, $\kappa = 3$ (- - -). (b) Mean intermolecular distances R_{TTA} for TTA, R_M for DMF, R_E for DEF; R_0 is the contact distance, R_{eff} the effective Smoluchowski distance for TTA. All curves refer to $R_{eff}(223\text{ K}) = 0.400\text{ nm}$, $\kappa = 2$.

the greatest deviations from the solid curve. Within an accuracy of ± 0.02 of the experimental values of Q_{EM} , all eight theoretical curves are acceptable. In Fig. 10b the following quantities referring to $\kappa = 2$, $R_{eff} = 0.40\text{ nm}$ are shown: The mean radius R_{TTA} of TTA, the effective Smoluchowski radius R_{eff} for TTA, and the mean radii R_E for DEF and R_M for DMF.

6. Discussion

Further development and testing of the kinetic model will depend on the reliability and completeness of experimental values of the intensity ratio Q_{EM} and on the availability of auxiliary experimental data: (1) experimental values of Q_{EM} in the low-temperature range between 110 and 133 K; (2) auxiliary experimental data related to TTA and delayed fluorescence; (3) data on the prompt excimer fluorescence of fluoranthene. In the following we discuss first the significance of these desirable, additional or auxiliary experimental data, then some aspects of the kinetic model, and finally some aspects of the DEF spectrum.

6.1 Completeness and reliability of experimental values of Q_{EM}

The present experimental values of the intensity ratio Q_{EM} of DEF and DMF are not yet completely satisfactory. At low temperatures, the uncertainty of ± 2 K in the absolute temperature become serious. Moreover, a small systematic error in the measurement of the temperature cannot be excluded with certainty ($T_{true} < T_{meas}$ – cf. the item *Sample* in Sect. 2). The uncertainty of the absolute temperature can be reduced from ± 2 K to ± 0.1 K by using a suitable cryostat [42]. This would simultaneously allow one to measure Q_{EM} down to 110 K. The measurement of Q_{EM} can be made much faster by measuring the spectra of delayed fluorescence and prompt fluorescence with a CCD camera. An absolute accuracy of ± 0.02 for Q_{EM} should be attainable in the whole temperature range from 110 to 300 K. A principal difficulty in the determination of Q_{EM} is discussed in Sect. 6.5 below.

The experimental determination of Q_{EM} is based on the assumption that the spectra of DMF and prompt monomer fluorescence (PMF) are identical, if polarization effects are eliminated. This assumption is certainly justified for high temperatures, where the excimer-monomer equilibrium is established during the lifetime of the excited state. Polarization effects were not explicitly eliminated, because their influence on the spectrum of the prompt fluorescence was negligible in the covered temperature range: From the polarization of the short-lived fluorescence of biphenylene in 3-methylpentane [43] we conclude that the orientational relaxation time of fluoranthene at the lowest temperature was $\lesssim 1$ ns, i.e. much shorter than the lifetime of S_1 (53 ns). With decreasing temperature, however, the mean radius for DMF, R_M , decreases and asymptotically approaches the mean radius for TTA, R_{TTA} (see Fig. 10). The curve $R_M(T)$ has a minimum at 112 K, which should correspond to a maximum difference between the spectra of PMF and DMF. This offers an independent test of the kinetic model. Small but significant differences between the spectra of PMF and DMF have been known since long (e.g. for anthracene and perylene [16]), but there has been no systematic investigation of this effect.

6.2 Auxiliary experimental data related to TTA and delayed fluorescence

The mean radius R_{TTA} of TTA in viscous solutions can be determined by a completely different experimental method, which is based on the initial anti-Smoluchowski time dependence of the delayed fluorescence after pulsed excitation [26, 27]. Wilhelm [34] studied the anti-Smoluchowski time dependence of the delayed fluorescence of fluoranthene in a 1 : 1 mixture of methylcyclohexane (MCH) and methylcyclopentane (MCP) in the temperature range from 105 K to 115 K, which corresponds to the temperature range from ≈ 102 K to ≈ 109 K of 3-methylpentane with respect to the ratio T/η [25]. The most reliable value of R_{TTA} of fluoranthene in MCH/MCP is $R_{TTA}(107.5 \text{ K}) = 1.53 \text{ nm}$

(r_a in Table 4.3 of [34]). At the equivalent temperature of 3-methylpentane (104.3 K), $R_{\text{TTA}} = 1.30$ nm. We discuss this result further in Sect. 6.4.

An important assumption of the kinetic model is the proportionality of the diffusion coefficient to T/η . In principle the absolute value of the diffusion coefficient of molecules in the triplet state can be measured in the whole temperature range of interest [33, 44, 45]. The effective Smoluchowski radius R_{eff} of TTA [39] can be measured in a large temperature range.

6.3 On the observability of prompt excimer fluorescence

In the following we shall show that the present positive results on excimer formation of fluoranthene are not in contradiction to the negative result reported by Berلمان *et al.* [12, 13], and we will suggest the detection of prompt excimer fluorescence by kinetic experiments.

The kinetic model yields an excimer-monomer equilibrium constant $K_{\text{EM}}^{(1)}$,

$$K_{\text{EM}}^{(1)} = p_{\text{E}}^{(1)} / p_{\text{M}}^{(1)} \equiv (1 - p_{\text{M}}^{(1)}) / p_{\text{M}}^{(1)} \quad \text{or} \quad p_{\text{M}}^{(1)} = (1 + K_{\text{EM}}^{(1)})^{-1}, \quad (6-1)$$

where the superscript (1) again indicates that the equilibrium refers to a single ground-state molecule in the finite volume V per solute molecule at a given concentration c_1 . The concentration dependence of K_{EM} can be derived as follows. Let n solute molecules instead of one be in the volume V . The probability $p_{\text{M}}^{(n)}$ that none of the n ground-state molecules is associated with the excited molecule is $p_{\text{M}}^{(n)} = (p_{\text{M}}^{(1)})^n$. (The association of the excited molecule ${}^1\text{M}^*$ with more than one ground-state molecule ${}^1\text{M}$ is admitted; with the present definition of the contact radius R_0 , the association of one ${}^1\text{M}^*$ with two ${}^1\text{M}$ is physically possible.) The complementary probability that the excited molecule is associated with one or more ground-state molecules is $p_{\text{E}}^{(\geq 1)} = 1 - p_{\text{M}}^{(n)}$. The equilibrium constant referring to n molecules in the volume V is

$$K_{\text{EM}}^{(n)} = p_{\text{E}}^{(\geq 1)} / p_{\text{M}}^{(n)} = (1 + K_{\text{EM}}^{(1)})^n - 1, \quad (6-2)$$

where $n = c_n / c_1$. For small concentrations c_n the binomial expansion of Eq. (6-2) yields the expected proportionality between c_n and $K_{\text{EM}}^{(n)}$:

$$K_{\text{EM}}^{(n)} \approx K_{\text{EM}}^{(1)} n = K_{\text{EM}}^{(1)} (c_n / c_1). \quad (6-3)$$

The value of $K_{\text{EM}}^{(1)}$ at room temperature is $K_{\text{EM}}^{(1)}(298 \text{ K}) = 6.3 \cdot 10^{-5}$ ($R_{\text{eff}} = 0.40$ nm, $\kappa = 2$ – cf. Fig. 9 and Table 1). The corresponding concentration dependence according to Eqs. (6-2) and (6-3) is shown in Fig. 11.

Berلمان *et al.* [12] studied the concentration dependence of the fluorescence from fluoranthene in cyclohexane; up to a concentration of ≈ 0.069 mol dm $^{-3}$ they did not find any indication of excimer formation. If one assumes that the stability of the fluoranthene excimer is in cyclohexane about the same as in 3-methylpentane (although one should expect a lower stability

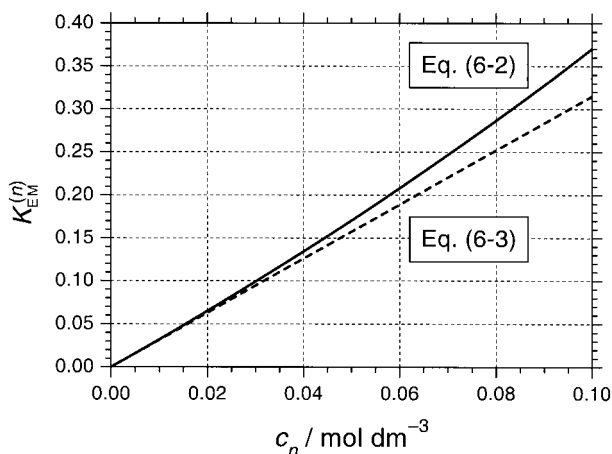


Fig. 11. Predicted concentration dependence of the excimer-monomer equilibrium constant $K_{EM}^{(n)}$ of fluoranthene in 3-methylpentane at 298 K, according to Eq. (6-2) (solid curve) and Eq. (6-3) (dashed line); $n = c_n/c_1$ and $c_1 = 2 \cdot 10^{-5} \text{ mol dm}^{-3}$. The saturation concentration of fluoranthene in 3-methylpentane at room temperature is $c_{\text{sat}} \approx 0.09 \text{ mol dm}^{-3}$.

of the excimer in the better solvent cyclohexane), then, according to Fig. 11 and at a concentration $\approx 0.069 \text{ mol dm}^{-3}$, about 80% of the total fluorescence should be monomer fluorescence and 20% excimer fluorescence. Because of the great similarity of the spectra of monomer and excimer fluorescence that means that virtually no excimer fluorescence should be spectroscopically detectable, in agreement with the negative statement made by Berlman *et al.* [12]. The same negative statement applies to fluoranthene in 3-methylpentane. At the saturation concentration of fluoranthene in 3-methylpentane at room temperature, $c_{\text{sat}} \approx 0.09 \text{ mol dm}^{-3}$, about 25% of the prompt fluorescence should be excimer fluorescence.

Nevertheless it should be possible to verify excimer formation by measuring the time dependence of the prompt fluorescence. Kinetically, reversible excimer formation is a complex phenomenon [46–48] (for the pertinent literature cf. the recent papers by Naumann on reversible excimer formation in particular [47] and on reversible fluorescence quenching in general [48]). For the present rough estimate, however, Birks' conventional treatment of the problem in terms of rate constants for excimer formation and dissociation is completely sufficient [6, 49]. According to this treatment, the time dependence of the prompt fluorescence should be approximately biexponential, if a considerable fraction of the total fluorescence is emitted as excimer fluorescence. In the present case, monomer-excimer equilibration is roughly 100 times faster than the decay of the fluorescence. In this case the general equations describing the time dependence of monomer and excimer fluorescence (cf. Chapt. 7.3

in [49]) simplify to

$$I_{\text{PMF}} \approx C_{\text{PMF}} \Phi_{\text{MF}} \left[{}^1\text{M}^* \right]_{t=0} \left(p_{\text{E}}^{\text{eq}} \exp(-\lambda_2 t) + p_{\text{M}}^{\text{eq}} \exp(-\lambda_1 t) \right), \quad (6-4)$$

$$I_{\text{PEF}} \approx C_{\text{PEF}} \Phi_{\text{EF}} \left[{}^1\text{M}^* \right]_{t=0} p_{\text{E}}^{\text{eq}} \left(-\exp(-\lambda_2 t) + \exp(-\lambda_1 t) \right), \quad (6-5)$$

where C_{PMF} and C_{PEF} are constants depending on the fluorescence wavelength, $\Phi_{\text{MF}} = k_{\text{M}}^{\text{rad}}/k_{\text{M}}$, $\Phi_{\text{EF}} = k_{\text{E}}^{\text{rad}}/k_{\text{E}}$ (cf. Sect. 5.4), and p_{M}^{eq} and $p_{\text{E}}^{\text{eq}} = 1 - p_{\text{M}}^{\text{eq}}$ are equilibrium probabilities at the given concentration. The rate constants λ_1 and λ_2 are

$$\lambda_1 \approx p_{\text{M}}^{\text{eq}} k_{\text{M}} + p_{\text{E}}^{\text{eq}} k_{\text{E}}, \quad (6-6)$$

$$\lambda_2 \approx k_{\text{diss}} + k_{\text{ass}} = k_{\text{diss}} \left(1 + K_{\text{EM}}^{(n)} \right). \quad (6-7)$$

The best and the only reliable experimental proof of excimer formation would be the observation of a fast component in the 0-0 transition of the monomer fluorescence of fluoranthene. For the more viscous solvent cyclohexane (cf. Sect. 5.4) one would expect a fast component with a slightly concentration-dependent λ_2 of the order of 1 ns^{-1} and a relative amplitude that is approximately proportional to the ground-state concentration. With a time resolution of about 1 ns of the experimental technique used by Berlman and coworkers [50] it was not possible to detect a fast component with a small relative amplitude. Therefore the observed concentration independence of the lifetime and the quantum yield of the fluorescence from fluoranthene can mean either that no excimer is formed (as assumed by Berlman *et al.* [12, 13]) or that incidentally the rate constants for radiative and nonradiative decay of the excimer are equal to those of the excited monomer (as assumed in Sect. 5.4 and in agreement with the reported lifetime of the excimer fluorescence from amorphous films of fluoranthene [36]). With time-correlated single photon counting it should be possible to detect reliably the fast fluorescence component due to monomer-excimer equilibration. Once the existence of the predicted fast component is beyond doubt, careful measurements of the concentration dependence of λ_1 and λ_2 and of the relative amplitude of the fast component should enable the determination of the equilibrium constant K_{EM} and the verification of the approximate equalities $k_{\text{E}} = k_{\text{M}}$ and $k_{\text{E}}^{\text{rad}} = k_{\text{M}}^{\text{rad}}$, postulated in Sect. 5.4.

6.4 Discussion of the kinetic model

Geminate excimer formation and dissociation cannot be treated by classical chemical kinetics in terms of rate constants. In principle, molecular dynamics should offer the best approach to the kinetic treatment of geminate excimer formation. In practice, however, molecular dynamics cannot be applied for two

reasons. First, of the required bimolecular interaction potentials and distance- and orientation-dependent rate coefficients, seven are unknown and cannot be easily estimated: ${}^3\text{M}^* \dots {}^3\text{M}^*$ interaction potential and orientation and distance dependence of TTA, ${}^1\text{M}^* \dots {}^1\text{M}$ interaction potential and orientation and distance dependence of radiative and nonradiative decay of the excited singlet state, and the interaction potentials of ${}^3\text{M}^*$, ${}^1\text{M}^*$, and ${}^1\text{M}$ with the solvent. Second and more importantly, a molecular dynamics simulation cannot be extended to times of the order of $1 \mu\text{s}$. Therefore a kinetic treatment based on a Smoluchowski equation like the present one is a good compromise. (For a more detailed discussion of kinetic models based on the Smoluchowski equation cf. the Conclusions in a recent paper by Solntsev and Agmon [51] on a geminate diffusion-influenced reaction).

A very unsatisfactory feature of the present kinetic model is connected with the choice of the contact radius R_0 . The radial probability densities of the ${}^3\text{M}^* \dots {}^3\text{M}^*$ and ${}^1\text{M}^* \dots {}^1\text{M}$ distribution functions are assumed to be proportional to r^2 also in the radial range $R_0 \leq r \leq R_{\text{av}}$. Physically this assumption makes no sense with nonspherical molecules. Let the fluoranthene molecule be approximated by an oblate rotational ellipsoid with a short diameter $2a$, a long diameter $2b$, a shortest contact distance $R_0 = 2a$ and an average diameter $R_{\text{av}} = 2(ab^2)^{1/3}$. Let one ellipsoid be spatially fixed and let the space angle $\Omega_1(r)$ characterize the admissible directions for the center of the second molecule at the distance r from the center of the first molecule. Let the space angle $\Omega_2(\theta, r)$ characterize the possible orientations of the second molecule at the distance r from the first molecule and in a direction with an angle θ relative to the short axis of the first ellipsoid. Three distance ranges and two singular points can be distinguished: (a) $2b \leq r$, $\Omega_1 = 4\pi$, $\Omega_2 = 4\pi$; (b) $a + b \leq r < 2b$, $\Omega_1 = 4\pi$, $\Omega_2(\theta, r) \leq 4\pi$; (c) $2a < r < a + b$, $\Omega_1 < 4\pi$, $\Omega_2(\theta, r) < 4\pi$; (d) $r = 2a$, $\theta = 0$ or π , $\Omega_1 = 0$, $\Omega_2 = 0$. Thus, in the present treatment, small values of r close to R_0 are strongly overrated. In particular the equilibrium distribution $\rho_S(r)_{\text{eq}}$ has a maximum at R_0 , whereas $\rho_S(R_0)_{\text{eq}} = 0$ would be correct according to the preceding consideration.

The arbitrary choice of the excimer potential function might be considered to be the weakest point of the kinetic model. The fact, however, that rather different potential functions (cf. Table 1) yield very similar functions $Q_{\text{EM}}(T)$ (see Fig. 10a), implies that the choice of the potential type $U(r)$ is not critical. Conversely that means that the potential depth $U(R_0)$, the halfwidth Γ , and the mean distance R_{E} for excimer fluorescence have no direct physical meaning.

The third rather unsatisfactory feature of the kinetic model is the arbitrary distance dependence of the relative diffusion coefficient D . Fortunately, the specific form of $D(r)$ is not essential in the excimer range $R_0 \leq r \leq R_0 + \Gamma$. In the whole temperature range, where a DEF can be observed with certainty, and at times $\geq 0.01/k_S$, the distribution function $\rho_S(r, t)$ in the range $R_0 \leq r \leq R_0 + \Gamma$ is almost exactly proportional to the equilibrium distribu-

tion $\rho_S(r)_{\text{eq}}$ (see Fig. 7). Moreover, also the probability for TTA in that radial range is small even at the highest temperature (see the values of $p_{E0}(0)$ in Fig. 8).

In conclusion, as far as the radial near zone $R_0 \leq r \lesssim 2R_0$ is concerned, the kinetic model is an essentially empirical description. The physically meaningful quantities are the singlet distribution function $\rho_S(r, t)$ for $r \gtrsim 2R_0$ in the time range of interest, the probabilities $p_E(t)$ and $p_M(t)$ for the excimer and the excited monomer, the mean radii R_{TTA} for TTA and R_M for monomer fluorescence, the equilibrium constant $K_{\text{EM}}^{(1)}$, the excimer binding enthalpy B_E , and the dissociation rate constant k_{diss} .

Perhaps the most important assumption in the application of the kinetic model is the value of the Smoluchowski radius for TTA, $R_{\text{eff}}(223 \text{ K}) = 0.40 \text{ nm}$. The variation of R_{eff} by $\pm 0.05 \text{ nm}$ (see Table 1) roughly corresponds to the achievable accuracy in experimental determinations of R_{eff} [39]. By the choice of $R_{\text{eff}}(223 \text{ K})$ the range of admissible values of the contact radius R_0 is automatically restricted. For instance, with $R_0 = 0.75 \text{ nm}$ and $\kappa = 2$, a function $Q_{\text{EM}}(T)$ very similar to the functions $Q_{\text{EM}}(T)$ in Fig. 10a can be computed, but there is no parameter combination that yields $R_{\text{eff}}(223 \text{ K}) = 0.40 \text{ nm}$. In other words, if the contact radius R_0 is treated as a free parameter, then the maximum of R_0 , compatible with $R_{\text{eff}}(223 \text{ K}) = 0.40 \text{ nm}$, is close to the present fixed value $R_0 = 0.35 \text{ nm}$.

It has not been possible to find a satisfactory kinetic description for the whole temperature range. The present theoretical curves for Q_{EM} in Figs. 3 and 10a were optimized for the temperature range from the maximum of Q_{EM} up to room temperature. The rather steep drop of the experimental values of Q_{EM} at low temperatures could mean that the distance dependence of the first-order TTA rate constant k_{1A} is not approximately exponential in the range from 0.4 to 1.2 nm, where TTA essentially takes place (see Fig. 6 and 10b).

The application of the kinetic model may seem doubtful at high viscosities, where the steady-state triplet distribution $\rho_T(r, \infty)$ is not even approximately reached. In practice, however, this implies no serious restriction to the range of validity of the kinetic model. On the one hand, the triplet lifetime strongly increases with increasing viscosity (up to a maximum of $\approx 0.7 \text{ s}$ [34]). On the other hand, in the radial near zone, where TTA takes place, $\rho_T(r, t)$ become almost exactly proportional to $\rho(r, \infty)$, when the absolute value of $\rho_T(r, t)$ still strongly differs from $\rho_T(r, \infty)$ [27].

More sophisticated kinetic models are conceivable within the limitations imposed by the spherical approximation. In particular the effect of spin statistics on TTA, which leads to the magnetic-field dependence of the delayed fluorescence, can be taken into account [52, 53]. In this connection a triplet-triplet interaction potential can be included that depends on the total spin of a triplet pair. The hard-sphere approximation can be relaxed. A temperature dependence of all excited-state decay rate constants can be easily included in the kinetic model.

6.5 Spectrum of the excimer fluorescence and ground-state dimers

If the excimer fluorescence were a transition from a bound excited dimer to a completely unstable ground-state dimer, then the relative Stokes shift of the excimer fluorescence should be greater than the effective binding enthalpy $E_B \approx -hc \times 800 \text{ cm}^{-1}$ of the excimer. The relative Stokes shift of the excimer fluorescence at 153 K is $(\Delta\tilde{\nu})_{\text{Stokes}} = -420 \text{ cm}^{-1}$. A different estimate of the Stokes shift can be based on the fact that the spectrum of the DEF looks like a broadened and slightly red-shifted spectrum of the PMF. In Fig. 12 three spectra are compared: the spectra of the DEF and the PF and a third spectrum denoted by PF*. The PF* spectrum is obtained by convolution of the PF spectrum with a Gaussian

$$g(\tilde{\nu}') = (\pi\sigma^2)^{-1/2} \exp(-(\tilde{\nu}'/\sigma)^2), \quad (6-8)$$

which accounts for additional inhomogeneous broadening in a dimer, and by an additional red-shift $(\Delta\tilde{\nu})_{\text{red}}$ of the convoluted spectrum. By fitting the PF* spectrum to the DEF spectrum between 16000 and 22000 cm^{-1} , $\sigma = 590 \text{ cm}^{-1}$ and $(\Delta\tilde{\nu})_{\text{red}} = -300 \text{ cm}^{-1}$ were obtained (wavenumbers were varied in steps of 10 cm^{-1}). The PF* spectrum virtually coincides with the DEF spectrum

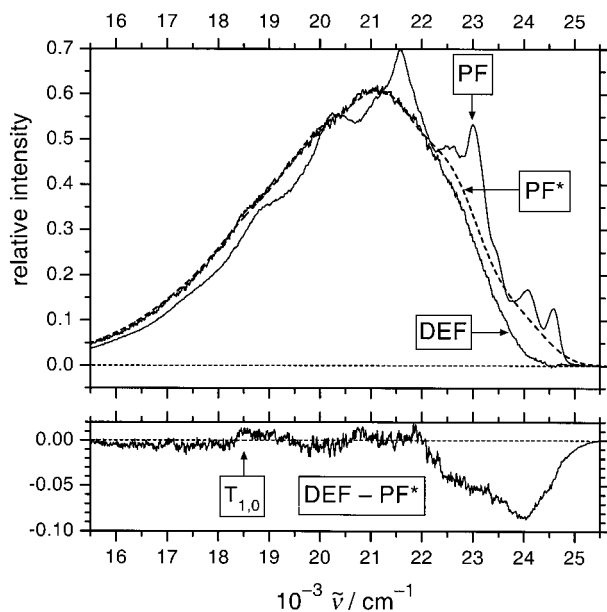


Fig. 12. Spectra of the prompt fluorescence (PF) and DEF (multiplied by 1.9406) of fluoranthene at 153 K (from Fig. 2). The spectrum PF* was calculated from the spectrum PF by convolution with a Gaussian of halfwidth 818 cm^{-1} (fwhm) and a red-shift of 300 cm^{-1} (fit range from 16000 to 22000 cm^{-1}).

between 15 500 and 22 000 cm^{-1} , but exhibits significant deviations from the DEF spectrum at higher wavenumbers. In particular the relative contribution of the 0-0 transition to the DEF spectrum seem to be by an order of magnitude weaker than expected. This result can be rationalized as follows. Crystalline fluoranthene is monoclinic [54]. The unit cell contains eight molecules, which are grouped in four head-to-tail dimers. If the excimer of fluoranthene has also a head-to-tail sandwich configuration, then the lowest excimer state and the electronic ground state are g states with a forbidden electronic transition between them [55–57]. Therefore, essentially only nontotally symmetric vibronic transitions contribute to the excimer fluorescence of fluoranthene. It is known that nontotally symmetric vibronic transitions strongly dominate in the monomer fluorescence of fluoranthene. The $S_1 \rightarrow S_0$ transition in fluoranthene is inherently very weak [58, 59] and gains most of its vibronic intensity by vibronic coupling with higher excited singlet states. With jet-cooled isolated fluoranthene molecules the strongest vibronic transitions refer to false origins [60].

Relative to the PF^* spectrum, the lacking intensity in the DEF spectrum amounts to -5.4% . The difference spectrum of PF^* and DEF does not sensitively depend on the definition of the DEF spectrum. For instance, if in Fig. 2 the PF spectrum is multiplied by 0.97, the value of the intensity ratio increases Q_{EM} of DEF and DMF increases by $\approx 6\%$, but the difference spectrum remains qualitatively the same; only the amplitude of the minimum at 24 000 cm^{-1} reduces from ≈ -0.085 to ≈ -0.075 . (This uncertainty in the choice of the difference spectrum limits the attainable accuracy of Q_{EM} in the maximum of $Q_{\text{EM}}(T)$.) The rough equality of the DEF spectrum with an inhomogeneously broadened and slightly red-shifted PMF spectrum supports the assumption that the rate constants for the radiative and total decay of the excimer are approximately equal to those of the excited monomer.

The binding enthalpy B_G of the ground-state dimer can be estimated as proposed by Döller and Förster (cf. Eq. (9) in [61]):

$$B_G \approx B_E - hc(\Delta\tilde{\nu})_{\text{red}} \approx hc \times (-800 + 300) \text{ cm}^{-1} = -hc \times 500 \text{ cm}^{-1}. \quad (6-9)$$

With respect to the observability of prompt excimer fluorescence (PEF), postulated in Sect. 6.2, this estimate implies a restriction. If part of the PEF results from the excitation of ground-state dimers, the kinetic detection of excimer formation becomes more difficult, because the relative amplitude of the fast component becomes smaller. On the other hand, it should be possible to vary the relative amplitude by varying the excitation wavelength. In particular the expected strong splitting of the $S_0 \rightarrow S_4$ transition (at 34 800 cm^{-1} , see Fig. 1) in the dimer offers the possibility of almost selective monomer excitation at 34 800 cm^{-1} .

6.6 Terminology: Excited dimer versus excimer

Although the word *excimer* results from the contraction of the words *excited* and *dimer* [62], the terms *excited dimer* and *excimer* have not been used as synonyms in the literature. The introduction of the term excimer by Stevens and Hutton in 1960 [62] was based on the misinterpretation of the delayed excimer fluorescence of pyrene (TTA as the cause of delayed fluorescence had not yet been discovered in 1960; the slow decay of the DEF was attributed to an extremely long radiative lifetime of the excimer). According to their original definition, an *excited dimer* is produced by the excitation of a ground-state dimer whereas an *excimer* is produced by the secondary association of an excited monomer with a ground-state molecule. The main disadvantage of this definition of the two terms is that the required knowledge of the stability of the corresponding ground-state dimer is in general not available. The alternative definition of the two terms is based on the fluorescence spectrum: The spectrum of an excimer is structureless and completely different from the fluorescence spectrum of the monomer, whereas the fluorescence spectrum of an excited dimer is similar to the fluorescence spectrum of the monomer. The obvious disadvantage of the alternative definition is the existence of borderline cases. In practice the term *excimer* has been applied to all kinds of more or less structureless fluorescence that is emitted by assemblies of two or more molecules, such as the fluorescence from amorphous thin films of aromatic hydrocarbons [36, 63] or of polymers. This practice is not objectionable since the term *excimer* can be formed also by contracting one of the terms *excited trimer*, *excited tetramer*, or *excited polymer*. On the other hand, the explicit term *excited dimer* should be only used when the presence of higher aggregates can be excluded with certainty. The distinctive feature of the delayed excimer fluorescence from dilute solutions of aromatic hydrocarbons is that the fluorescence from higher aggregates than dimers can be excluded with certainty. In the present paper we dispensed with the distinction between the two terms, in agreement with the recommendation made by Barashkov *et al.* (cf. Sect. VIII in [5]).

7. Conclusions

(1) The delayed fluorescence from a dilute solution of fluoranthene ($2 \cdot 10^{-5}$ mol dm⁻³) in 3-methylpentane at low temperatures consists of two components: delayed monomer fluorescence (DMF) and a slightly red-shifted component, which is assigned to delayed excimer fluorescence (DEF).

(2) The ratio Q_{EM} of the spectrally integrated intensities of DEF and DMF exhibits the type of temperature dependence, which is expected for a weakly bound excimer. $Q_{EM}(T)$ has a maximum at ≈ 150 K and decreases almost to zero at room temperature.

(3) At the maximum of $Q_{EM}(T)$, the rise and the decay of the delayed fluorescence are consistent with the presence of a single triplet species. The

observation of the rise of the delayed fluorescence becomes possible by the chopping the excitation beam with two choppers with very different chop frequencies.

(4) The temperature dependence of the intensity ratio $Q_{EM}(T)$ can be described with a kinetic model that is based on a Smoluchowski equation. The basic features of the kinetic model are: a distance-dependent relative diffusion coefficient, an exponential distance dependence for the annihilation of a triplet pair, and the representation of the excimer by a short-range attractive potential. The hard-sphere contact distance is assumed to be equal to the intermolecular distance in a sandwich excimer (0.35 nm).

(5) The agreement of fitted theoretical curves with the experimental data is good in the temperature range from room temperature down to the maximum of $Q_{EM}(T)$.

(6) The kinetic model permits a prediction on the observability of prompt excimer fluorescence. In the 0-0 transition of the prompt fluorescence from a saturated solution of fluoranthene ($\approx 0.09 \text{ mol dm}^{-3}$) in 3-methylpentane at 298 K, the monomer-excimer equilibration should result in a fast component of the fluorescence decay at the 0-0 transition of the monomer fluorescence with a relative amplitude of about 0.3.

(7) The convolution of the spectrum of the prompt fluorescence (PF) at 153 K with a Gaussian of halfwidth (fwhm) 818 cm^{-1} and a red-shift of 300 cm^{-1} yields a PF* spectrum that almost exactly agrees with the DEF spectrum between $15\,500$ and $22\,000 \text{ cm}^{-1}$. At higher wavenumbers the DEF spectrum is below the PF* spectrum; in particular the 0-0 transition is virtually absent in the DEF spectrum. A head-to-tail arrangement of the two molecules in the excimer is proposed, with a forbidden 0-0 transition from the lowest excimer *g*-state to the ground state of the dimer.

(8) Fluoranthene in 3-methylpentane forms a ground-state dimer with a dimerization enthalpy of $\approx -hc \times 500 \text{ cm}^{-1}$.

Acknowledgement

We thank Professor Jürgen Troe for generous support, Dr. Wolfgang Naumann for discussions on diffusion-influenced reactions and the analytic treatment of some problems in the kinetics of triplet-triplet annihilation, Andreas vom Schloss for preliminary experiments on the delayed excimer fluorescence of fluoranthene, and Helmut Lesche for technical assistance.

References

1. J. B. Birks and L. G. Christophorou, *Prod. Roy. Soc. A* **277** (1964) 571.
2. B. Stevens and M. I. Ban, *Trans. Faraday Soc.* **60** (1964) 1515.
3. T. Förster, *Excimere*, *Angew. Chem.* **81** (1969) 364.
4. J. B. Birks, *Excimers*, *Rep. Prog. Phys.* **38** (1975) 903.

5. N. N. Barashkov, T. V. Sakhno, R. N. Nurmukhametov, O. A. Khakhel', *Excimers of organic molecules*, Usp. Khim. (Russ.) **62** (1993) 579 [Russ. Chem. Rev. **62** (1993) 539].
6. K. A. Zachariasse, *Kinetics and thermodynamics of excimer formation. Excited state equilibria*, Trends in Photochemistry & Photobiology **3** (1994) 211.
7. O. A. Khakhel', R. N. Nurmukhametov and T. V. Sakhno, Chem. Phys. Lett. **247** (1995) 185.
8. V. E. Krikunova, S. A. Serov and O. A. Khakhel', Opt. Spektrosk. (Russ.) **86** (1999) 427 [Opt. Spectrosc. **86** (1999) 373].
9. A. Warshel and E. Huler, Chem. Phys. **6** (1974) 463.
10. B. Stevens and J. T. Dubois, Trans. Faraday Soc. **62** (1966) 1525.
11. J. B. Birks and S. Georghiou, J. Phys. B (Proc. Phys. Soc.) Ser. 2 **1** (1968) 958.
12. I. B. Berlman, H. O. Wirth and O. J. Steingraber, J. Am. Chem. Soc. **90** (1968) 566.
13. I. B. Berlman, J. Phys. Chem. **74** (1970) 3085.
14. C. A. Parker and C. G. Hatchard, Trans. Faraday Soc. **59** (1963) 284.
15. C. A. Parker, *Photoluminescence of solutions*, Elsevier, Amsterdam (1968).
16. B. Nickel, Helv. Chim. Acta **61** (1978) 198.
17. B. Nickel and M. F. Rodríguez Prieto, Ber. Bunsenges. Phys. Chem. **92** (1988) 1493.
18. C. A. Parker, Nature **200** (1963) 331.
19. J. B. Birks, B. N. Srinivasan and P. S. McGlynn, J. Mol. Spectr. **27** (1968) 266.
20. B. Stevens and M. I. Ban, Mol. Cryst. **4** (1968) 173.
21. P. R. Butler and M. J. Pilling, J. Chem. Soc. Faraday II **73** (1977) 886.
22. B. Nickel and D. Klemp, Chem. Phys. **174** (1993) 297.
23. B. Nickel and G. Roden, Chem. Phys. **53** (1980) 243.
24. J. Hertzberg and B. Nickel, Chem. Phys. **132** (1989) 235.
25. A. A. Ruth, B. Nickel and H. Lesche, Z. Phys. Chem. **175** (1992) 91.
26. B. Nickel, H. E. Wilhelm and A. A. Ruth, Chem. Phys. **188** (1994) 267.
27. B. Nickel, H. E. Wilhelm and C. P. Jaensch, Opt. Spektrosk. (Russ.) **83** (1997) 584 [Opt. Spectrosc. **83** (1997) 541].
28. M. v. Smoluchowski, Z. Phys. Chem. **92** (1917) 129.
29. S. A. Rice, *Diffusion-Limited Reactions*, Vol. 25 of the series *Comprehensive Chemical Kinetics*, ed. C. H. Bamford, C. F. H. Tipper and R. G. Compton, Elsevier, Amsterdam (1985).
30. A. A. Ovchinikov, S. F. Timashev and A. A. Belyi, *Kinetics of Diffusion-Controlled Chemical Processes*, Nova, Commack (1989), (Russian original: Moscow, Khimiya, 1986).
31. M. v. Smoluchowski, Phys. Z. **17** (1916) 585.
32. S. H. Northrup and J. T. Hynes, J. Chem. Phys. **71** (1979) 871.
33. E. G. Meyer and B. Nickel, Z. Naturforsch. **35a** (1980) 503.
34. H. Wilhelm, *Anti-Smoluchowski-Zeitverlauf der verzögerten Fluoreszenz aromatischer Verbindungen*, Dissertation, Universität Göttingen 1995, Cuvillier Verlag, Göttingen (1995).
35. H. Güsten and G. Heinrich, J. Photochem. **18** (1982) 9.
36. W. Arden, L. M. Peter and G. Vaubel, J. Lumin. **9** (1974) 257.
37. R. Bonneau, J. Faure and J. Jousot-Dubien, Chem. Phys. Lett. **2** (1968) 65.
38. F. Tvibel and L. Lindqvist, Chem. Phys. **10** (1975) 471.
39. K. H. Grellmann and H.-G. Scholz, Chem. Phys. Lett. **62** (1979) 64.
40. B. Nickel, Z. Phys. Chem. **214** (2000) 753.
41. W. H. Press, B. P. Flannery, S. A. Teukolsky and W. T. Vetterling, *Numerical Recipes – The Art of Scientific Computing (FORTRAN Version)*, Cambridge University Press, Cambridge (1989).
42. B. Nickel and A. A. Ruth, J. Phys. Chem. **95** (1991) 2027.

43. B. Nickel and J. Hertzberg, *Chem. Phys.* **132** (1989) 219.
44. B. Nickel, *Ber. Bunsenges. Phys. Chem.* **76** (1972) 582.
45. B. Nickel and U. Nickel, *Ber. Bunsenges. Phys. Chem.* **76** (1972) 584.
46. M. N. Berberan-Santos and J. M. G. Martinho, *J. Chem. Phys.* **95** (1991) 1817.
47. W. Naumann, *J. Chem. Phys.* **111** (1999) 2414.
48. W. Naumann, *J. Chem. Phys.* **112** (2000) 7152.
49. J. B. Birks, *Photophysics of aromatic molecules*, Wiley-Interscience, London (1970).
50. O. J. Steingraber and I. B. Berlman, *Rev. Sci. Instr.* **34** (1963) 524.
51. K. M. Solntsev and N. Agmon, *Chem. Phys. Lett.* **320** (2000) 262.
52. J. Spichtig, H. Bulska and H. Labhart, *Chem. Phys.* **15** (1976) 279.
53. K. Lendi, P. Gerber and H. Labhart, *Chem. Phys.* **18** (1976) 449.
54. A. C. Hazell, D. W. Jones and J. M. Sowden, *Acta Cryst. B* **33** (1977) 1516.
55. Th. Förster, *Delocalized excitation and excitation transfer*, in *Modern Quantum chemistry, Part III: Action of light and organic crystals*, ed. O. Sinanoglu, Academic Press, New York (1965), p. 93–137.
56. S. P. McGlynn, A. T. Armstrong and T. Azumi, *Interaction of molecular exciton, charge resonance states, and excimer luminescence*, in *Modern Quantum chemistry, Part III: Action of light and organic crystals*, ed. O. Sinanoglu, Academic Press, New York (1965), p. 203–228.
57. M. Kasha, *Molecular excitons in small aggregates*, in *Spectroscopy of the excited state*, ed. B. Di Bartolo, Plenum Publ. Corp., New York (1976), p. 337–363.
58. J. Kolc, E. W. Thulstrup and J. Michl, *J. Am. Chem. Soc.* **96** (1974) 7188.
59. J. V. Goodpaster, J. F. Harrison and V. L. McGuffin, *J. Phys. Chem. A* **102** (1998) 3372.
60. I. Y. Chan and M. Dantus, *J. Chem. Phys.* **82** (1985) 4771.
61. E. Döller and Th. Förster, *Z. Phys. Chem. N. F.* **34** (1962) 132.
62. B. Stevens and E. Hutton, *Nature* **186** (1960) 1045.
63. D. R. Haynes, K. R. Helwig, N. J. Tro, S. M. George, *J. Chem. Phys.* **93** (1990) 2836.